Journal of Applied Physics

RESEARCH ARTICLE | NOVEMBER 09 2022

High electron mobility in AlN:Si by point and extended defect management

Pegah Bagheri ✉; Cristyan Quiñones-Garcia; Dolar Khachariya; ... et. al

Journal of Applied Physics 132, 185703 (2022)
https://doi.org/10.1063/5.0124589

AIP Publishing

Journal of Applied Physics ARTICLE scitation.org/journal/jap

High electron mobility in AlN:Si by point and extended defect management

Cite as: J. Appl. Phys. **132**, 185703 (2022); doi: 10.1063/5.0124589
Submitted: 7 September 2022 · Accepted: 18 October 2022 ·
Published Online: 9 November 2022

View Online Export Citation CrossMark

Pegah Bagheri,[1,a)] Cristyan Quiñones-Garcia,[1] Dolar Khachariya,[2] Shashwat Rathkanthiwar,[1] Pramod Reddy,[2] Ronny Kirste,[2] Seiji Mita,[2] James Tweedie,[2] Ramón Collazo,[1] and Zlatko Sitar[1,2]

AFFILIATIONS

[1]Department of Materials Science and Engineering, North Carolina State University, Raleigh, NC 27695, USA
[2]Adroit Materials, Cary, NC 27518, USA

[a)]**Author to whom correspondence should be addressed:** pbagher@ncsu.edu

ABSTRACT

High room temperature n-type mobility, exceeding 300 cm^2/Vs, was demonstrated in Si-doped AlN. Dislocations and C_N^{-1} were identified as the main compensators for AlN grown on sapphire and AlN single crystalline substrates, respectively, limiting the lower doping limit and mobility. Once the dislocation density was reduced by the growth on AlN wafers, C-related compensation could be reduced by controlling the process supersaturation and Fermi level during growth. While the growth on sapphire substrates supported only high doping ($[Si] > 5 \times 10^{18}\ cm^{-3}$) and low mobility (~20 cm^2/Vs), growth on AlN with proper compensation management enabled controlled doping at two orders of magnitude lower dopant concentrations. This work is of crucial technological importance because it enables the growth of drift layers for AlN-based power devices.

INTRODUCTION

Single crystal aluminum nitride with a direct bandgap of 6.1 eV and high Debye temperature brings about technological opportunities to realize deep UV optoelectronics, extreme RF, and power devices in addition to being an ideal host for quantum interaction.[1–6] Implementation of AlN as a semiconductor can lead to a revolution in power electronics due to its high breakdown field (greater than 15 MV/cm) and the possibility of high temperature operation.[7] In order to realize AlN-based devices, doping and compensation must be managed in the entire range of doping levels from Si concentration of 10^{17} to $10^{20}\ cm^{-3}$. This doping range generates technologically relevant carrier concentrations and mobilities required for the various layers that makeup diodes, transistors, LEDs, and LDs, such as drift, contact, and cladding layers.[2,8] Si and Ge are the n-type dopants of choice in $Al_xGa_{1-x}N$ $(0 \le x \le 1)$ where they behave as shallow donors for $x < 0.8$ and $x < 0.5$, respectively.[9–11] However, an hypothesized donor transition to the DX^{-1} acceptor state, thought to be the cause of the high donor ionization energy in Al-rich AlGaN and AlN, puts a fundamental limitation on the practicality of the AlN-based devices.[12] This is based on the fact that the DX^{-1} acts as a self-compensating defect, pinning the Fermi level within the gap, making the free electron concentration independent of both doping concentration and growth conditions. However, there has been no direct evidence for existence of DX^{-1} in nitrides. Recently, Bagheri *et al.* provided direct proof of single electron occupancy for donors in Al-rich AlGaN and AlN.[13] In other words, donors are stable in a deeper donor state (D^0) in Al-rich AlGaN and AlN, exhibiting a high ionization energy. This makes controllable n-type doping via epitaxy in AlN feasible, however, it requires proper point defect management due to a large excess energy available for the generation of compensating point defects. Generally, doping in AlGaN across the whole composition range shows a characteristic "knee" behavior, where the electron concentration does not generally follow a one to one ratio with the dopant concentration.[14–16] At the low-doping-limit, compensation by C_N and dislocations limits the minimum controllable dopant concentration along with the maximum mobility.[17] The enhancement in carrier concentration and mobility via suppression of C_N incorporation has been reported before for Si and Ge doped GaN and AlGaN.[17–23] In contrast, on the high doping side, the formation of metal vacancy-related point defects determines the maximum achievable carrier concentration.[24,25] Both doping ranges are required for the realization of either high mobility drift layers or conductive contact layers.

The incorporation of point defects in III-Ns varies significantly by changing the growth environment and can be successfully managed by the universal defect management toolbox established by Reddy *et al.*, where the point defects' formation energy is related to the MOCVD growth "knobs" (Chemical Potential Control—CPC) or Fermi level position (Defect Quasi Fermi Level Control—dQFL).[26,27] Orders of magnitude enhancement in maximum achievable carrier concentration and mobility have been demonstrated for Ge and Si-doped GaN and AlGaN of various compositions.[15,18,19,24,28] However, attempts to realize controllable n-type doping and to extend the doping limits in AlN for various applications are still in their infancy. Like any other effective doping, controllable n-type doping in AlN requires low dislocation density and identification and management of any compensating point defects.

In this work, a roadmap for management of C_N^- and dislocation-related compensation during the growth of Si-doped AlN is described. The implementation of the CPC and dQFL methods led to more than one order of magnitude reduction in the minimum controllable dopant concentration along with the demonstration of state-of the art mobility of 300 cm^2/Vs at an electron concentration of 10^{15} cm^{-3} in AlN:Si. This work represents a crucial step toward the achievement of AlN-based high power and high frequency electronics.

EXPERIMENTAL

AlN films were grown on c-oriented sapphire wafers and AlN single crystal substrates in a vertical, low-pressure (20 Torr), RF-heated, cold-walled MOCVD reactor. Trimethylaluminum (TMA) and ammonia were used as aluminum and nitrogen precursors, respectively. Growth on the sapphire substrate started with 7 min of H_2 etching at 1100 °C and 4 min of nitridation under NH_3 at 950 °C. A low temperature, the AlN nucleation layer (20 nm) was deposited at 650 °C and then annealed at 1050 °C for 15 min, followed by the growth of a 200 nm thick AlN layer at 1200 °C that served as an Al-polar AlN template. This template was annealed under N_2 at 760 Torr and 1700 °C for 1 h, providing a low dislocation density template.[29,30] AlN single crystal substrates had a dislocation density $<10^3$ cm^{-2}. Details on the surface preparation and epitaxial growth on AlN single crystal substrates are described elsewhere.[31–33] Subsequently, a 500 nm thick unintentionally doped AlN layer, followed by a 500 nm thick Si-doped AlN layer were grown on both types of substrates, using silane as the Si precursor (0.1 and 1 ppm in nitrogen). The dopant concentration was varied between 5×10^{17} and 5×10^{19} cm^{-3}. Doped AlN layers were grown under H_2 diluent, at 1100, 1300, and 1400 °C and V/III ratios of 1000, 3000, and 6000. These V/III ratios were achieved by changing of NH_3 flow rate from 0.3 to 3 slm and Al flow rate from 14 to 7 μmol/min. Correspondingly, the growth rate was reduced from 500 to 125 nm/h. A Hg lamp was used during the growth as the above-bandgap illumination source with an optical power of 1 W/cm^2 to generate minority carriers.[19] The dislocation density in the films on the AlN template ($\sim 10^9$ cm^{-2}) and AlN single crystal substrate ($<10^3$ cm^{-2}) were estimated from x-ray diffraction (XRD) measurements using a Philips X'Pert materials research diffractometer with a Cu anode and x-ray topography.[34,35] All doped films showed smooth surfaces with RMS roughness <1 nm, as observed by atomic force microscopy. Electrical characterization was performed using temperature-dependent Hall measurements (8400 series Lakeshore AC/DC Hall system) in the van der Pauw configuration from 200 to 1000 K. Prior to measurements, V/Al/Ni/Au (30/100/70/70 nm) stacks were deposited as contacts by electron beam evaporation. Contacts were annealed at 850 °C for 1 min via rapid thermal annealing.

RESULTS AND DISCUSSION

Carbon and dislocations were shown to be the main compensators determining the low-doping-limit in GaN.[18] Dislocations act as acceptor-type compensators with an equivalent concentration proportional to their density,[36]

$$N_A \propto \frac{TDD}{|\vec{c}|}. \quad (1)$$

As such, for a typical dislocation density in AlN grown on sapphire and on AlN substrates, N_A can be estimated as low as mid-10^{18} and $\sim 10^{11}$ cm^{-3}, respectively.[36] Carbon is another species with a negative charge state in n-type III-Ns that can act as a compensator and has been shown to cause mobility collapse.[18,24] Interestingly, C_N incorporation can be managed during the growth where a N-richer growth environment and application of above-bandgap illumination were shown to increase its formation energy.[18,19,24,27]

C_N formation energy in AlN depends on the chemical potentials of nitrogen (μ_N), carbon (μ_C), and the Fermi level position with respect to the valence band (E_F–E_V) as per Eq. (2),[37]

$$\Delta E^f(C_N^-) = \Delta\mu_N - \Delta\mu_C - 2[E_F + E_V]. \quad (2)$$

Gaddy *et al.*[38] calculated the formation energy of C_N in AlN under N- and III-rich growth conditions as shown in Fig. 1. The reference formation energies were calculated in Gaddy *et al.*,[38] and Fig. 1 is an illustration of CPC and dQFL methods. The use of the CPC method for C_N management in AlN is based on the increase in the process supersaturation (σ), leading to a higher μ_N, as shown in Fig. 1(a). In this study, the process supersaturation was increased either by increasing the V/III ratio and reactor pressure or decreasing the total metal organic flow rate.[20,24] As for the dQFL control, minority carriers were generated by above-bandgap illumination to shift the quasi-Fermi level position during the growth away from the conduction band as shown in Fig. 1(b). This in turn increased the C_N^- formation energy, leading to a decrease in compensation by this defect. Details on the CPC and dQFL methods are described elsewhere.[26,27] The following paragraphs discuss the room temperature carrier concentration and mobility for AlN films with high and low dislocation density, grown on sapphire, and AlN single crystalline substrates, respectively (Fig. 2), for varying chemical potentials, accessed by varying the V/III ratio or growth temperature (Figs. 3 and 4), and for various Fermi levels achieved by minority carrier generation during growth (Fig. 5). Figures 2–5 use the same scale for ease of comparison.

The effect of dislocations on doping is summarized in Fig. 2. The viable doping range for AlN on sapphire substrates with dislocation density $\sim 10^9$ cm^{-2} is narrow (5×10^{18}–3×10^{19} cm^{-3}) compared to the homoepitaxial growth, which supports more than one

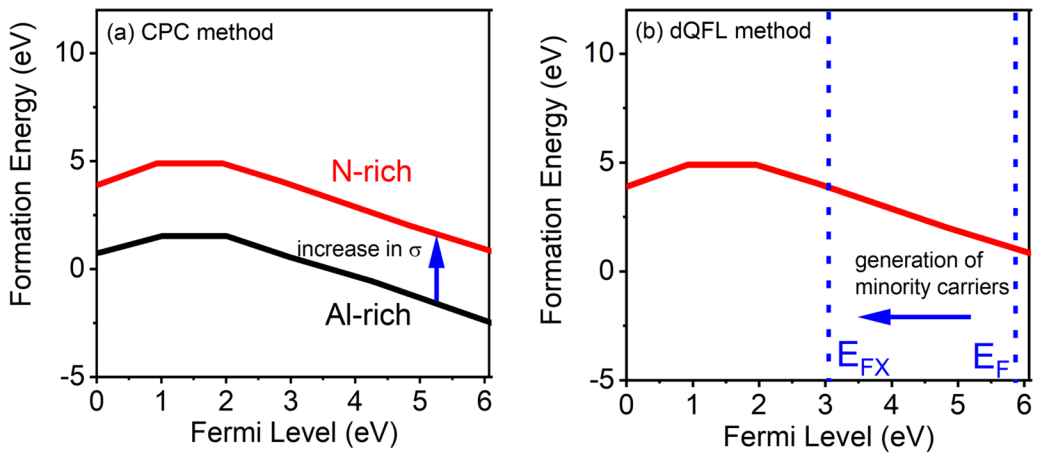

FIG. 1. Calculated C_N formation energy in AlN under N-rich and Al-rich growth conditions based on Gaddy *et al.*[38] and demonstration of (a) CPC and (b) dQFL methods as the components of defect management toolbox in III-N.

order of magnitude lower controllable doping levels at the same growth conditions. A lower low-doping-limit is crucial for the development of AlN-based high-voltage power electronics. Doped AlN films with high dislocation density grown on sapphire showed the characteristic knee behavior, where the drop in carrier concentration and mobility after the knee is attributed to the formation of V_{III}–nSi_{III} complexes.[24,28] On the other hand, the low-doping-limit, characterized by a drop in the mobility with decreasing [Si], occurred for sapphire substrates already for $[Si] \lesssim 10^{19}\,cm^{-3}$. The dashed black arrows in Fig. 2 point to the [Si] where the films became too resistive to measure. Interestingly, no measurable conductivity was achieved in Si-doped AlN on sapphire substrates below $5 \times 10^{18}\,cm^{-3}$ under any growth conditions. Clearly, dislocations are in these samples the main compensating acceptor centers, limiting the maximum mobility to $\sim 20\,cm^2/Vs$ and carrier concentration to $\sim 1 \times 10^{15}\,cm^{-3}$. Clearly, controllable doping range can be extended to the lower levels only if the dislocations are removed. As shown in Fig. 2, Si-doped films grown on AlN single crystalline substrates with low dislocation density showed two times higher free electron concentration along with a factor of 2 higher mobility ($40\,cm^2/Vs$).

Figure 3 summarized the effect of V/III ratio on carrier concentration and mobility. A twofold increase in the mobility to $80\,cm^2/Vs$ was achieved on AlN substrates by increasing the V/III ratio from 1000 to 3000, leading to a decrease in $[C_N^-]$.[20]

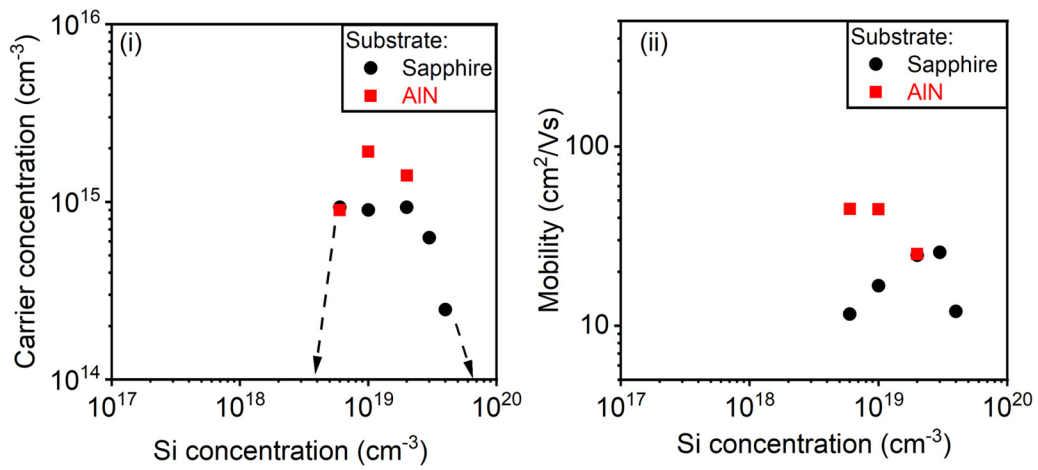

FIG. 2. Room temperature variation of (i) carrier concentration and (ii) mobility as a function of [Si] on sapphire (DD $\sim 10^9\,cm^{-2}$) and AlN single crystal (DD $\sim 10^3\,cm^{-2}$) substrates. All films were grown at a V/III ratio of 1000 and growth temperature of 1100 °C. Dashed arrows pointed to the [Si] where electrical measurements were not possible.

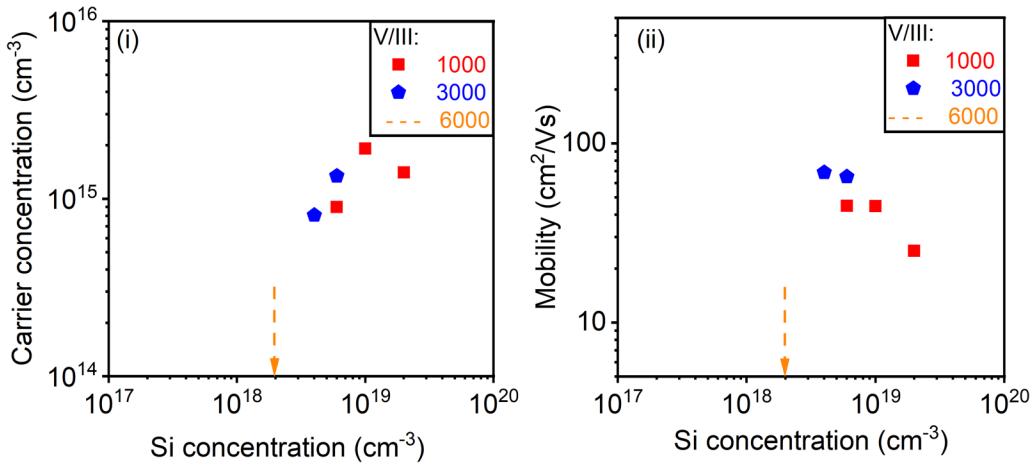

FIG. 3. Room temperature variation of (i) carrier concentration and (ii) mobility with [Si] under V/III ratios of 1000, 3000, and 6000 at a growth temperature of 1100 °C on the AlN single crystal substrate. Dashed arrows point to the [Si] where electrical measurements were not possible.

Simultaneously, the carrier concentration increased more than fourfold due to the reduction in charge compensators. Further reduction in the [Si] at these V/III ratios was not expected to improve mobility since C_N seemed to be the main scattering center. A further increase of the V/III ratio and reduction of [Si] to $\sim 2 \times 10^{18}$ cm^{-3} (dashed orange arrow) leads to highly resistive films as at these conditions [C_N^-] is above [Si_{Al}^+]. It is important to note that CPC is effective only when [C_N^-] can be maintained below the dopant concentration.

Figure 4 shows a strong impact of growth temperature on the electrical properties of Si-doped AlN. A significant increase in the mobility (>300 cm^2/Vs) and a reduction of the lower doping limit (<10^{18} cm^{-3}) was demonstrated by increasing the growth temperature to 1300 °C. As shown previously, an increase in the growth temperature produces N-richer growth, i.e., increases μ_N, and decreases the incorporation of C_N.[24] Interestingly, there seems to exist a critical growth temperature where any further increase of growth temperature (dashed brown arrow at 1400 °C) results in semi-insulting behavior. The formation of V_{Al} and Si complexes is more likely at higher growth temperatures, resulting in highly resistive films.[24] Therefore, the choice of growth temperature is a compromise between the minimization of [C_N] and management of the concentration of V_{Al}-related defects below the [Si]. It is important to note that this critical temperature can be shifted higher if the V_{Al}-related defects can be managed by other process input parameters.

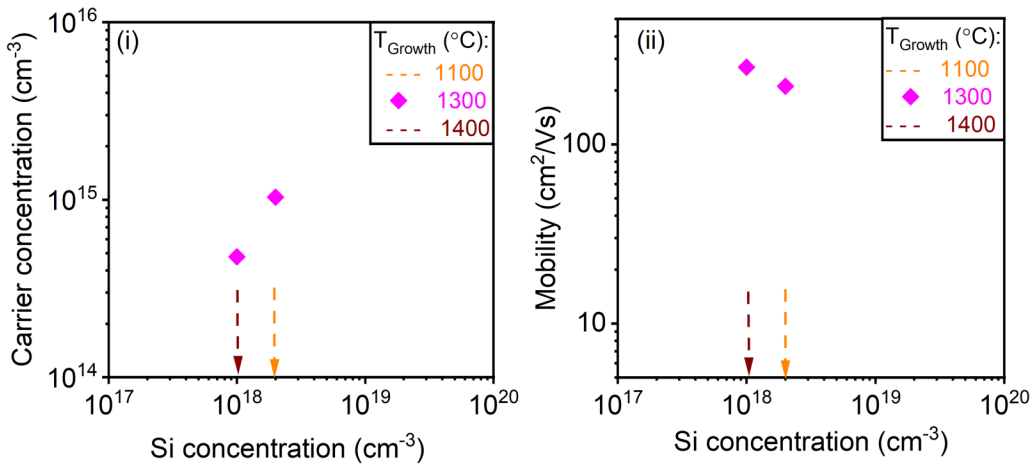

FIG. 4. Room temperature variation of (i) carrier concentration and (ii) mobility with [Si] under a V/III ratio of 6000 and growth temperatures of 1000, 1300, and 1400 °C on AlN single crystal substrate. Dashed arrows point to the [Si] where electrical measurements were not possible.

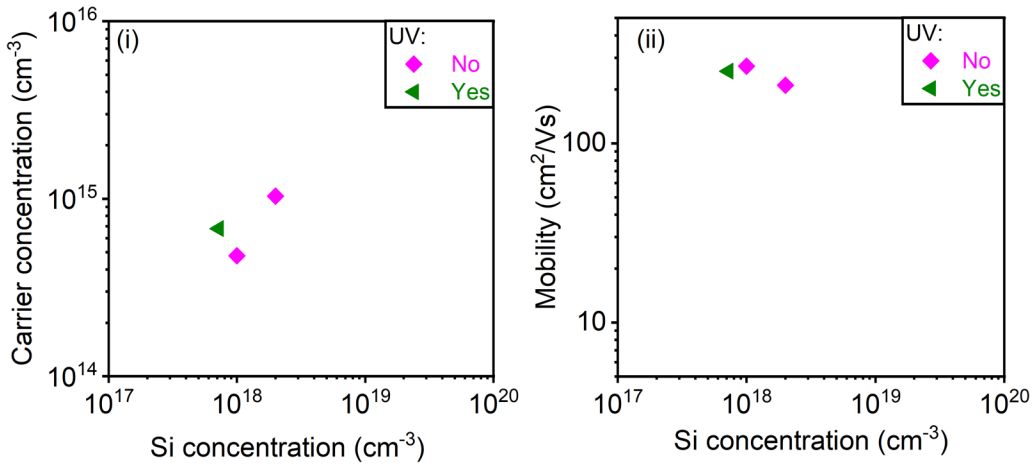

FIG. 5. Room temperature variation of (i) carrier concentration and (ii) mobility with [Si] grown at 1300 °C and a V/III ratio of 6000 with and without above-bandgap illumination on the AlN single crystal substrate.

Finally, the impact UV illumination as a component of the dQFL method is shown in Fig. 5. A decrease of [Si] under the same growth condition but with the UV illumination showed about twofold increase in carrier concentration. Generation of minority carriers during growth[27] (in this case via above-bandgap illumination) can further increase the formation energy of C_N^-, reduce compensation, and allow for a lower low-doping-limits. A mobility of 300 cm^2/Vs was measured for samples grown under above-bandgap illumination and doped at [Si]~7×10^{17} cm^{-3}.

Based on the results and discussion above, it is clear that the chosen growth conditions influence compensation through thermodynamics. To quantify the compensation as a function of growth conditions, temperature-dependent carrier concentration and mobility were investigated. The variation of electron concentration with temperature was described using the charge balance model: $n = [Si^+] - [N_A^-]$, where N_A^- represents all acceptor-type compensators. Ionization of Si with temperature follows the Fermi-Dirac statistics and $[N_A^-] = [N_A]$ due to the full ionization of the acceptors in an n-type semiconductor.[39] Therefore, the carrier concentration is obtained as

$$n = \frac{[\mathrm{Si}]}{1 + \frac{g_{Si}}{N_C(T)} n \exp\left(\frac{\Delta E_{Si}}{k_B T}\right)} - [\mathrm{N_A}]. \quad (3)$$

Here, g_{Si} is the degeneracy factor (assumed 2 for donors), $N_C(T) = 1.2 \times 10^{15} T^{1.5} (\mathrm{cm}^{-3})$ is the AlN conduction band effective density of states, and ΔE_{Si} is the ionization energy of Si. It is worth noting that the charge balance model for n-type doping in AlN is valid only when the doping range does not favor the formation of V_{Al}–nSi_{Al} complexes. In the self-compensation regime, where complexes are energetically favorable to form, Si does not only incorporate in the donor state but also forms the complexes and $[\mathrm{Si}]_{\mathrm{total}} \neq [\mathrm{Si}]_{\mathrm{donor}}$. Therefore, we employ Eq. (3) only for [Si] < 10^{19} cm^{-3}, where self-compensation is low compared to [Si].[25] Figure 6 shows the temperature-dependent Hall measurement and a fitting curve based on Eq. (3) for Si-doped AlN grown at 1100 °C, under V/III ratio of 3000 and [Si]~3×10^{18} cm^{-3}. ΔE_{Si} and $[N_A]$

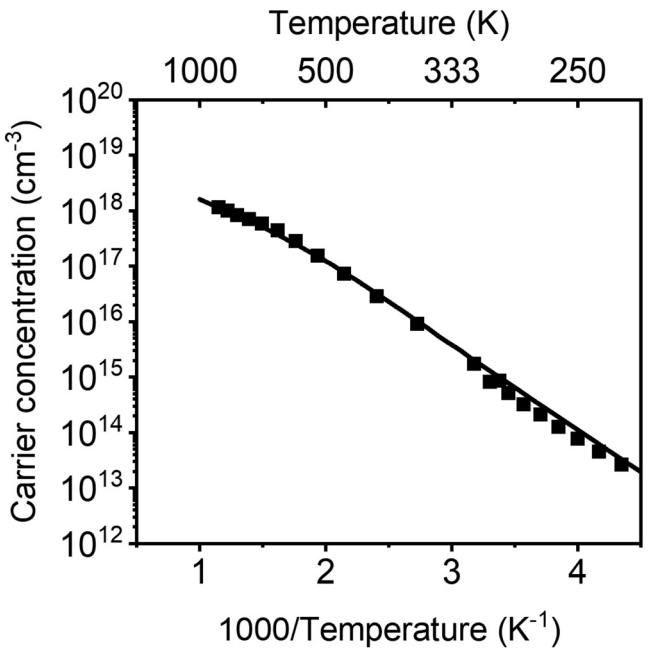

FIG. 6. Temperature-dependent hall measurements for carrier concentration in Si-doped AlN grown at 1100 °C under a V/III ratio of 3000 and [Si]~3×10^{18} cm^{-3} on the AlN substrate. The fitting curve is based on Eq. (3) with ΔE_{Si} and $[N_A]$ as fitting parameters. The confidence interval of fitting is better than 99%.

were used as fitting parameters. Si ionization energy was extracted to be 260 ± 10 meV which is in agreement with values reported in the literature.[40,41] Temperature-dependent Hall on all samples showed very similar behavior (not shown here) with different carrier concentrations at elevated temperatures exhibiting the role of compensation ratio (N_A/N_{Si}) under various growth conditions.

Mobility dependence on temperature was investigated to determine the effect of various scattering centers. The mobility was modeled following the Matthiessen's rule:

$$\mu_{Total}^{-1} = \mu_{II}^{-1} + \mu_N^{-1} + \mu_{dis}^{-1} + \mu_{AP}^{-1} + \mu_{OP}^{-1} + \mu_{piez}^{-1}. \quad (4)$$

Equation (4) considers all possible scattering mechanisms in AlN, namely, ionized impurity (μ_{II}), neutral impurity (μ_N), dislocation (μ_{dis}), acoustic phonon (μ_{AP}), optical phonon (μ_{OP}), and piezoelectric scattering (μ_{piez}).[36,42] The dependence of each scattering mechanism on temperature is explained elsewhere.[36] Table I shows the AlN properties used to model the scattering mechanisms and evaluate the electron mobility at each temperature. In this model, Si ionization energy was assumed to be 260 meV as extracted from the charge balance model above. Dislocation densities were assumed to be 10^3 and 10^9 cm^{-2} for AlN and sapphire substrates, respectively. Carrier concentration was an experimental parameter (based on Hall measurement) and [ionized impurity] = $[Si^+] + [N_{II}^-]$ and [neutral impurity] = $[Si]-[Si^+]$ were calculated accordingly. Temperature-dependent electron mobility and the fitting curves are shown in Fig. 7 for various conditions. Here, N_{II} represented the concentration of all ionized point defects (excluding the ionized Si concentration) affecting the mobility and was the only fitting parameter. Interestingly, the technologically important room temperature mobility shows a strong impact of ionized impurity scattering (here, N_{II} and Si^+) and dislocations. Hence, extended and point defect management via low dislocation density native substrates and process supersaturation, respectively, effectively enhanced the mobility from <20 to >300 cm^2/Vs. The maximum mobility measured was 400 cm^2/Vs at 250 K in the sample grown at 1300 °C and a V/III ratio of 6000. High temperature mobilities are mostly limited by phonon scatterings and converge to similar values independent of the growth conditions, as shown in Fig. 7.

A comparison between N_A and N_{II} reveals the type of defect that is dominant in charge compensation and mobility scattering.

TABLE I. AlN properties used to model the scattering mechanisms for Eq. (4).[43,44]

Parameter	Values from the literature
Static dielectric constant	8.5
High frequency dielectric constant	4.8
Effective mass	0.4
Average longitudinal elastic constant	377.8 GPa
Average transversal elastic constant	134.5 GPa
Deformation potential	4.3 eV
Optical phonon energy	99.2 meV
Polar phonon Debye temperature	1151
Piezoelectric scattering constant[36]	2.63 C/m^2

The fitting parameter in the charge balance model, N_A, corresponds to all charged compensators including negatively charged point defects and dislocations (i.e., $N_A = N_{II} + N_{dis}$). However, the fitting parameter included in the mobility model (N_{II}) reflects only the role of charged point defects affecting the relaxation time. The

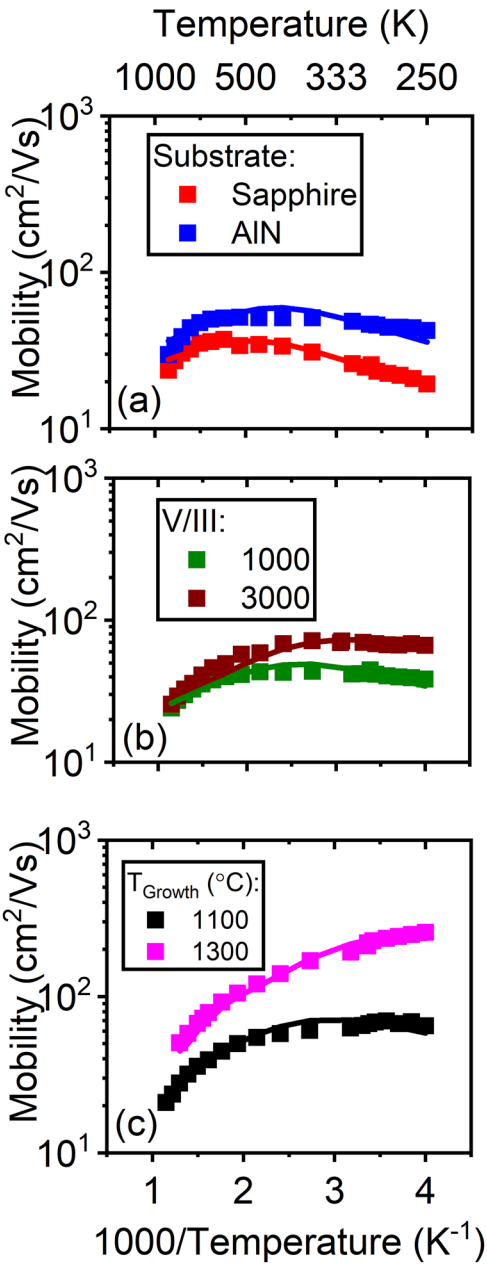

FIG. 7. Temperature-dependent mobility and fitting curves for various (a) substrates, (b) V/III ratios, and (c) growth temperatures in Si-doped AlN based on Eq. (4). The confidence interval of fitting is better than 99%. The fitting parameters are [N_{II}] for the mobility model representing charged point defects.

effect of dislocations is considered separately as μ_{dis}. Therefore, for a high dislocation density, AlN:Si, $N_A \neq N_{II}$, while $N_A \sim N_{II}$ if the dislocation density is negligible.

Figure 8 shows the effect of growth conditions on N_A and N_{II} as extracted from the charge balance and mobility models, respectively. The growth on sapphire showed one order of magnitude higher N_A than the growth on native AlN substrates under similar process conditions. In this case, compensation is dominated by dislocations acting as acceptor centers, where N_{dis} is in the mid-high 10^{18} cm^{-3} range while carbon results in $N_{II} \sim 10^{18}$ cm^{-3}, resulting in a net $N_A \sim 10^{19}$ cm^{-3}. Here, the dislocations are the main source of the compensating charge and the reason for low mobility in Si-doped AlN on sapphire.

In contrast, dislocation effects are practically eliminated on AlN substrates rendering $N_A \sim N_{II}$. In this case, N_A can be influenced significantly by process conditions, as shown in Fig. 8. As discussed at the beginning of this section, C_N is expected to be the main compensator at low dislocation density and its concentration decreases significantly by changing the process supersaturation. A sixfold increase in the V/III ratio and 200 °C increase in the growth temperature effectively reduced C_N (and both N_A and N_{II}) by more than one order of magnitude, from $\sim 10^{18}$ cm^{-3} to $<10^{17}$ cm^{-3}, resulting in mobilities above 200 cm^2/Vs as shown in Figs. 2–5. Finally, the implementation of above-bandgap illumination during growth (dQFL) further decreased N_A by a factor of 3 from 2×10^{17} to 6×10^{16} cm^{-3}, demonstrating state-of-the-art room temperature mobility for AlN of over 300 cm^2/Vs at a carrier concentration of 7×10^{14} cm^{-3}.

This work provided a systematic study to manage compensators in the low-doping regime (i.e., C_N) in Si:AlN to demonstrate high electron mobility for AlN-based power devices. Nevertheless, controllable n-type doping in highly Si-doped AlN via CPC and dQFL methods by managing the V_{Al}-nSi_{III} compensators can be another critical knob to enhance the free electron concentration in AlN for UV-LEDs and diodes.

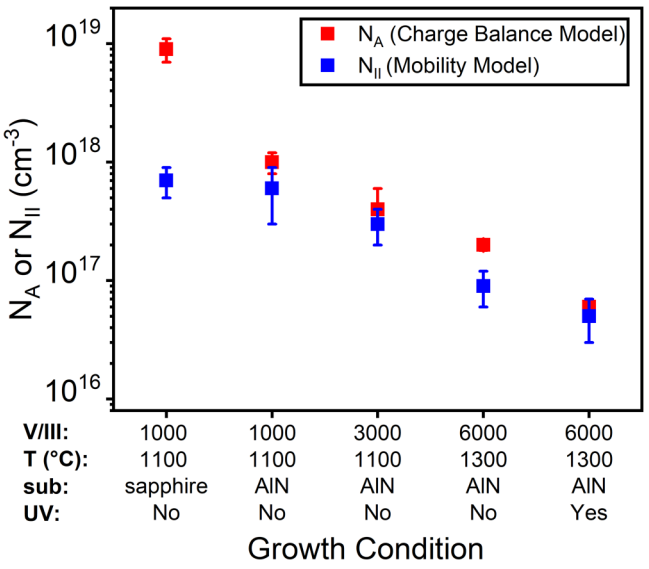

FIG. 8. N_A and N_{II} extracted from fitting curves based on Eqs. (3) and (4) in Figs. 6 and 7, respectively, for various growth conditions, substrates, and Fermi level management in Si-doped AlN. Error bars represent fitting results from multiple samples.

CONCLUSION

In conclusion, dislocations and incorporation of C severely limit n-doping and mobility in AlN. While dislocation density can be reduced by a factor of 10^6 by simply replacing sapphire substrates for single crystalline AlN, reduction in C incorporation requires a systematic approach in controlling process supersaturation and Fermi level during growth. It was shown that for AlN grown on sapphire, dislocations dominated the doping limits, while for the films with low dislocation density, it was controlled by ionized impurity scattering, i.e., C_N^{-1}. Following previously developed point defect control schemes,[26,27] the low–doping-limit was extended to [Si]~mid-10^{16} cm^{-3} with a state-of-the-art electron mobility exceeding 300 cm^2/Vs.

ACKNOWLEDGMENTS

The authors gratefully acknowledge funding in part from AFOSR (Nos. FA9550-17-1-0225 and FA9550-19-1-0114), DoD ARPA-E (No. DE-AR0001493), and NSF (Nos. ECCS-1508854, ECCS-1916800, and ECCS-1653383).

AUTHOR DECLARATIONS

Conflict of Interest

The authors have no conflicts to disclose.

Author Contributions

Pegah Bagheri: Conceptualization (lead); Data curation (lead); Formal analysis (lead); Investigation (lead); Methodology (lead); Writing – original draft (lead); Writing – review and editing (lead). **Cristyan Quiñones-Garcia** Data curation (supporting); Methodology (supporting). **Dolar Khachariya:** Data curation (supporting); Investigation (supporting); Methodology (supporting). **Shashwat Rathkanthiwar:** Formal analysis (supporting). **Pramod Reddy:** Formal analysis (supporting); Investigation (supporting); Methodology (supporting); Validation (equal); Writing – review and editing (equal). **Ronny Kirste:** Conceptualization (supporting). **Seiji Mita:** Conceptualization (equal); Data curation (equal). **James Tweedie:** Project administration (equal). **Ramón Collazo:** Funding acquisition (lead); Project administration (lead); Resources (lead); Supervision (lead); Validation (equal); Writing – review and editing (lead). **Zlatko Sitar:** Conceptualization (equal); Funding acquisition (lead); Investigation (equal); Project administration (lead); Resources (lead); Supervision (lead); Writing – review and editing (lead).

DATA AVAILABILITY

The data that support the findings of this study are available within the article.

REFERENCES

[1]H. Amano, R. Collazo, C. D. Santi, S. Einfeldt, M. Funato, J. Glaab, S. Hagedorn, A. Hirano, H. Hirayama, R. Ishii, Y. Kashima, Y. Kawakami, R. Kirste, M. Kneissl, R. Martin, F. Mehnke, M. Meneghini, A. Ougazzaden, P. J. Parbrook, S. Rajan, P. Reddy, F. Römer, J. Ruschel, B. Sarkar, F. Scholz, L. J. Schowalter, P. Shields, Z. Sitar, L. Sulmoni, T. Wang, T. Wernicke, M. Weyers, B. Witzigmann, Y.-R. Wu, T. Wunderer, and Y. Zhang, J. Phys. Appl. Phys. **53**, 503001 (2020).

[2]J. Y. Tsao, S. Chowdhury, M. A. Hollis, D. Jena, N. M. Johnson, K. A. Jones, R. J. Kaplar, S. Rajan, C. G. Van de Walle, E. Bellotti, C. L. Chua, R. Collazo, M. E. Coltrin, J. A. Cooper, K. R. Evans, S. Graham, T. A. Grotjohn, E. R. Heller, M. Higashiwaki, M. S. Islam, P. W. Juodawlkis, M. A. Khan, A. D. Koehler, J. H. Leach, U. K. Mishra, R. J. Nemanich, R. C. N. Pilawa-Podgurski, J. B. Shealy, Z. Sitar, M. J. Tadjer, A. F. Witulski, M. Wraback, and J. A. Simmons, Adv. Electron. Mater. **4**, 1600501 (2018).

[3]Y. Taniyasu, M. Kasu, and T. Makimoto, Nature **441**, 325 (2006).

[4]J. B. Varley, A. Janotti, and C. G. Van de Walle, Phys. Rev. B **93**, 161201 (2016).

[5]T.-J. Lu, B. Lienhard, K.-Y. Jeong, H. Moon, A. Iranmanesh, G. Grosso, and D. Englund, ACS Photonics **7**, 2650 (2020).

[6]T. Kinoshita, T. Nagashima, T. Obata, S. Takashima, R. Yamamoto, R. Togashi, Y. Kumagai, R. Schlesser, R. Collazo, A. Koukitu, and Z. Sitar, Appl. Phys. Express **8**, 061003 (2015).

[7]J. Xie, S. Mia, R. Dalmau, R. Collazo, A. Rice, J. Tweedie, and Z. Sitar, Phys. Status Solidi C **8**, 2407 (2011).

[8]R. Kirste, B. Sarkar, P. Reddy, Q. Guo, R. Collazo, and Z. Sitar, J. Mater. Res. **36**, 4638 (2021).

[9]P. Bagheri, R. Kirste, P. Reddy, S. Washiyama, S. Mita, B. Sarkar, R. Collazo, and Z. Sitar, Appl. Phys. Lett. **116**, 222102 (2020).

[10]B. J. Baliga, IEEE Electron Device Lett. **10**, 455 (1989).

[11]A. Bansal, K. Wang, J. S. Lundh, S. Choi, and J. M. Redwing, Appl. Phys. Lett. **114**, 142101 (2019).

[12]L. Gordon, J. L. Lyons, A. Janotti, and C. G. Van de Walle, Phys. Rev. B **89**, 085204 (2014).

[13]P. Bagheri, P. Reddy, S. Mita, D. Szymanski, J. H. Kim, Y. Guan, D. Khachariya, A. Klump, S. Pavlidis, R. Kirste, R. Collazo, and Z. Sitar, J. Appl. Phys. **130**, 055702 (2021).

[14]I. Bryan, Z. Bryan, S. Washiyama, P. Reddy, B. Gaddy, B. Sarkar, M. H. Breckenridge, Q. Guo, M. Bobea, J. Tweedie, S. Mita, D. Irving, R. Collazo, and Z. Sitar, Appl. Phys. Lett. **112**, 062102 (2018).

[15]K. Nagata, H. Makino, T. Yamamoto, K. Kataoka, T. Narita, and Y. Saito, Appl. Phys. Express **13**, 025504 (2020).

[16]S. Washiyama, K. J. Mirrielees, P. Bagheri, J. N. Baker, J.-H. Kim, Q. Guo, R. Kirste, Y. Guan, M. H. Breckenridge, A. J. Klump, P. Reddy, S. Mita, D. L. Irving, R. Collazo, and Z. Sitar, Appl. Phys. Lett. **118**, 042102 (2021).

[17]F. Kaess, S. Mita, J. Xie, P. Reddy, A. Klump, L. H. Hernandez-Balderrama, S. Washiyama, A. Franke, R. Kirste, A. Hoffmann, R. Collazo, and Z. Sitar, J. Appl. Phys. **120**, 105701 (2016).

[18]F. Kaess, P. Reddy, D. Alden, A. Klump, L. H. Hernandez-Balderrama, A. Franke, R. Kirste, A. Hoffmann, R. Collazo, and Z. Sitar, J. Appl. Phys. **120**, 235705 (2016).

[19]S. Rathkanthiwar, P. Bagheri, D. Khachariya, S. Mita, S. Pavlidis, P. Reddy, R. Kirste, J. Tweedie, Z. Sitar, and R. Collazo, Appl. Phys. Express **15**, 051003 (2022).

[20]S. Mita, R. Collazo, A. Rice, R. F. Dalmau, and Z. Sitar, J. Appl. Phys. **104**, 013521 (2008).

[21]D. D. Koleske, A. E. Wickenden, R. L. Henry, and M. E. Twigg, J. Cryst. Growth **242**, 55 (2002).

[22]A. Kakanakova-Georgieva, S.-L. Sahonta, D. Nilsson, X. T. Trinh, N. T. Son, E. Janzén, and C. J. Humphreys, J. Mater. Chem. C **4**, 8291 (2016).

[23]K. Ikenaga, A. Mishima, Y. Yano, T. Tabuchi, and K. Matsumoto, Jpn. J. Appl. Phys. **55**, 05FE04 (2016).

[24]S. Washiyama, P. Reddy, B. Sarkar, M. H. Breckenridge, Q. Guo, P. Bagheri, A. Klump, R. Kirste, J. Tweedie, S. Mita, Z. Sitar, and R. Collazo, J. Appl. Phys. **127**, 105702 (2020).

[25]J. S. Harris, J. N. Baker, B. E. Gaddy, I. Bryan, Z. Bryan, K. J. Mirrielees, P. Reddy, R. Collazo, Z. Sitar, and D. L. Irving, Appl. Phys. Lett. **112**, 152101 (2018).

[26]P. Reddy, S. Washiyama, F. Kaess, R. Kirste, S. Mita, R. Collazo, and Z. Sitar, J. Appl. Phys. **122**, 245702 (2017).

[27]P. Reddy, M. P. Hoffmann, F. Kaess, Z. Bryan, I. Bryan, M. Bobea, A. Klump, J. Tweedie, R. Kirste, S. Mita, M. Gerhold, R. Collazo, and Z. Sitar, J. Appl. Phys. **120**, 185704 (2016).

[28]P. Bagheri, J. H. Kim, S. Washiyama, P. Reddy, A. Klump, R. Kirste, S. Mita, R. Collazo, and Z. Sitar, J. Appl. Phys. **130**, 205703 (2021).

[29]S. Washiyama, Y. Guan, S. Mita, R. Collazo, and Z. Sitar, J. Appl. Phys. **127**, 115301 (2020).

[30]H. Miyake, G. Nishio, S. Suzuki, K. Hiramatsu, H. Fukuyama, J. Kaur, and N. Kuwano, Appl. Phys. Express **9**, 025501 (2016).

[31]A. Rice, R. Collazo, J. Tweedie, R. Dalmau, S. Mita, J. Xie, and Z. Sitar, J. Appl. Phys. **108**, 043510 (2010).

[32]R. Dalmau, B. Moody, R. Schlesser, S. Mita, J. Xie, M. Feneberg, B. Neuschl, K. Thonke, R. Collazo, A. Rice, J. Tweedie, and Z. Sitar, J. Electrochem. Soc. **158**, H530 (2011).

[33]I. Bryan, A. Rice, L. Hussey, Z. Bryan, M. Bobea, S. Mita, J. Xie, R. Kirste, R. Collazo, and Z. Sitar, Appl. Phys. Lett. **102**, 061602 (2013).

[34]J. Tweedie, R. Collazo, A. Rice, J. Xie, S. Mita, R. Dalmau, and Z. Sitar, J. Appl. Phys. **108**, 043526 (2010).

[35]B. Raghothamachar, R. Dalmau, B. Moody, H. S. Craft, R. Schlesser, J. Q. Xie, R. Collazo, M. Dudley, and Z. Sitar, Mater. Sci. Forum **717–720**, 1287 (2012).

[36]E. C. H. Kyle, S. W. Kaun, P. G. Burke, F. Wu, Y.-R. Wu, and J. S. Speck, J. Appl. Phys. **115**, 193702 (2014).

[37]C. Freysoldt, B. Grabowski, T. Hickel, J. Neugebauer, G. Kresse, A. Janotti, and C. G. Van de Walle, Rev. Mod. Phys. **86**, 253 (2014).

[38]B. E. Gaddy, Z. Bryan, I. Bryan, R. Kirste, J. Xie, R. Dalmau, B. Moody, Y. Kumagai, T. Nagashima, Y. Kubota, T. Kinoshita, A. Koukitu, Z. Sitar, R. Collazo, and D. L. Irving, Appl. Phys. Lett. **103**, 161901 (2013).

[39]K. Seeger, *Semiconductor Physics: An Introduction* (Springer Science & Business Media, 2013).

[40]R. Collazo, S. Mita, J. Xie, A. Rice, J. Tweedie, R. Dalmau, and Z. Sitar, Phys. Status Solidi C **8**, 2031 (2011).

[41]S. Contreras, L. Konczewicz, J. Ben Messaoud, H. Peyre, M. Al Khalfioui, S. Matta, M. Leroux, B. Damilano, and J. Brault, Superlattices Microstruct. **98**, 253 (2016).

[42]Y. Taniyasu, M. Kasu, and T. Makimoto, Appl. Phys. Lett. **89**, 182112 (2006).

[43]C. M. Lueng, H. L. W. Chan, C. Surya, and C. L. Choy, J. Appl. Phys. **88**, 5360 (2000).

[44]M. Kazan, E. Moussaed, R. Nader, and P. Masri, Phys. Status Solidi C **4**, 204 (2007).